Radiation-produced electron and hole centres in oxygen-containing BaFBr. II. An ENDOR study of O_F^-

1991 J. Phys.: Condens. Matter 3 9339

(http://iopscience.iop.org/0953-8984/3/47/007)

J. Phys.: Condens. Matter 3 (1991) 9339–9349. Printed in the UK

Radiation-produced electron and hole centres in oxygen-containing BaFBr: II. An ENDOR study of O_F^-

R S Eachus†, W G McDugle†, R H D Nuttall†, M T Olm†, F K Koschnick‡, Th Hangleiter‡ and J-M Spaeth‡

† Corporate Research Laboratories, Eastman Kodak Company, Rochester, NY 14650–2021, USA

‡ University of Paderborn, Fachbereich Physik, Warburger Strasse 100, 4790 Paderborn, Federal Republic of Germany

Received 29 July 1991

Abstract. Oxygen contamination introduces hole-trapping centres into barium fluorohalides. In the preceding paper, an O^- centre was reported as the product of the reaction between out-of-plane Br_2^- V_K centres and oxide impurities. This paper describes an ENDOR study of this centre which identifies it as O_F^-, an oxygen ion substituted at a fluoride site. No evidence has been found for the presence of a neighbouring defect (anion vacancy or interstitial cation) remaining from its charge-compensating role for the proposed precursor O_F^{2-}.

1. Introduction

Barium fluorobromide crystallizes with the PbFCl structure, as shown in figure 1 (Liebich and Nicollin 1977, Beck 1979). The nominally pure material is heavily coloured by x-radiation at room temperature, the result of the formation of F centres at bromide and fluoride sites and related species such as aggregates of F centres (Takahashi *et al* 1984, Takahashi *et al* 1985, von Seggern *et al* 1988). The properties of $F(Br^-)$ (Koschnick *et al* 1988) and $F(F^-)$ (Koschnick and Spaeth 1991) have been well characterized by ENDOR (electron nuclear double resonance) and ODMR (optically detected magnetic resonance) studies of both x-irradiated and additively coloured samples.

The nature of the hole centres formed simultaneously is a subject of active research and some conjecture, especially when the material is doped with rare-earth cations such as Eu^{2+}. Early suggestions (Takahashi *et al* 1984, Takahashi *et al* 1985, von Seggern *et al* 1988) that Eu^{2+} is converted to Eu^{3+} during x-radiation have been disputed (Eachus and Nuttall 1988, Trauernicht and Sever 1988, Hangleiter *et al* 1990, Spoonhower and Ahlers 1989). Previous studies have shown that V_K centres are the primary hole species formed during low temperature irradiation, but that these decay upon warming to room temperature (Eachus and Nuttall 1988, Hangleiter *et al* 1990). Concurrent with this decay, several stable, trapped-hole species are formed, but Eu^{3+} is not one of these. Two such centres, observed in a wide range of nominally pure and rare-earth-doped crystals and powders, are being assigned as oxygen-containing defects (Eachus *et al* 1991, 1991b).

0953-8984/91/479339+11$03.50

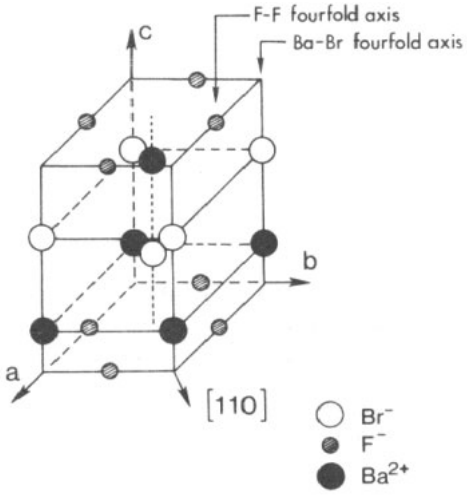

Figure 1. Crystal structure of BaFBr (Liebich and Nicollin 1977, Beck 1979).

This report describes results of structural studies of one of the oxygen-containing hole centres. We reported EPR measurements establishing that the central ion is oxygen in part I of this set of papers (Eachus et al 1991). A large increase in the radiation yield for this centre following deliberate O^{2-} addition and the observation of a single magnetic nucleus per centre in the ^{17}O enrichment experiments were reported. The following reaction sequence was inferred (Eachus *et al* 1991):

$$Br_2^- + [O^{2-} \cdot V_{Br-}] \rightarrow [O^- \cdot V_{Br-}] + 2Br^- \rightarrow O^- + V_{Br-} + 2Br^-$$

where V_{Br-} represents a bromide vacancy and $[O^{2-} \cdot V_{Br-}]$ represents a spatial correlation of the O^{2-} and the vacancy.

The purpose of this paper is to describe ENDOR experiments from which we have determined that the O^- ion is substituted for a lattice fluoride ion (O_F^-). The second centre, tentatively assigned to an O^- ion substitutional for a lattice bromide ion (O_{Br}^-), will be treated in a subsequent report (Eachus *et al* 1991b).

2. Experimental procedure

The EPR spectrometer and UV- and x-irradiation equipment have been described in Part I (Eachus *et al* 1991). X-band ENDOR spectra were measured on a highly modified Bruker ER200D EPR/ENDOR spectrometer equipped with a continuous flow helium cryostat. ENDOR measurements were generally carried out at 4.2 K with a cylindrical TM_{110} Bruker ENDOR/TRIPLE cavity and 10 mW of microwave power. The radiofrequency (RF) radiation was chopped at a rate of 10 KHz and the resulting ENDOR signal was phase-sensitive detected at the chopping rate. An RF power level of either 25 W or 6 W was used to obtain ENDOR spectra. The higher RF power level was necessary to detect first shell bromide ion ENDOR transitions, but gave rise to harmonics of the fluoride ENDOR transitions. The magnetic field was measured using a Bruker B–H15 NMR gaussmeter.

Optically detected ENDOR was measured as RF- and microwave-induced changes of the magnetic circular dichroism of the absorption (MCDA) with a custom built, computer controlled ODEPR/ODENDOR spectrometer working in K-band (24 GHz) and at 1.5 K (Ahlers *et al* 1982, Meyer *et al* 1982). The MCDA is the differential absorption of right- and left-polarized light.

ENDOR data accumulation and reduction was accomplished with an HP9000/550 computer. The data reduction software used baseline subtraction, digital filtering and resolution enhancement algorithms similar to those described by others (Niklas 1983, Spaeth 1989). A computer program which uses numerical diagonalization to solve the spin-Hamiltonian matrix for transition fields (EPR) and energies (ENDOR) and transition probabilities has been used to optimize parameters in the spin-Hamiltonian to fit observed transitions and to simulate spectra. This program has been described previously (Rinneberg and Weil 1972).

Sample preparation was described in Part I (Eachus *et al* 1991). Crystals grown in argon, carbon monoxide or a 9% mixture of hydrogen in argon gave the same results.

3. Results and site assignment

Undoped BaFBr crystals x-irradiated at room temperature for times ranging from 30 s to several hours yielded the EPR spectra, at 20 K or lower, shown in figure 2. The transitions shown arise from the defect that will be eventually assigned as O_F^-. The assignment to an oxygen-containing centre was based upon EPR and ODEPR experiments in which oxygen hyperfine splittings were observed in crystals doped with BaO enriched with the magnetic ^{17}O isotope (Eachus *et al* 1991).

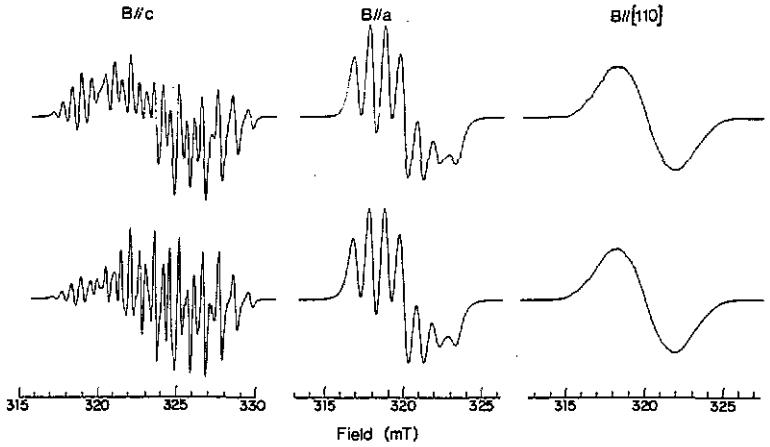

Figure 2. Experimental EPR spectra (9.15 GHz) of O_F^- in BaFBr x-irradiated 300 s at room temperature (upper curve) and spectra calculated using a spin-Hamiltonian which includes hyperfine interactions only with bromine (lower curve). Simulations used Lorentzian lineshapes and linewidths of 0.15, 0.35 and 0.45 mT, respectively.

The EPR spectra shown in figure 2 were measured with the magnetic field along the *a*, [110], or *c* directions as defined in figure 1. Although the structure changed on rotating the field from *a* to [110], the position of the multiplet was independent of the field orientation in the *ab* plane. A small field shift was observed on rotating

the field orientation from a position in the ab plane to c. No splittings assignable to the presence of more than one type of defect or more than one symmetry site for a given defect were detected. Thus, within the spectral resolution available with X-band EPR, the spectra in figure 2 arise from a single symmetry site for one type of defect. This has been confirmed by spectral simulations based on ENDOR results discussed below. The experimentally observed angular dependence was analysed to yield the g-matrix in table 1. Although the seven-line pattern observed with $\boldsymbol{B} \parallel a$ suggests a primary superhyperfine (SHF) interaction with two equivalent bromide ions, the angular variation of the SHF splittings was too complicated to allow a full analysis from EPR studies alone.

Table 1. Spin-Hamiltonian parameter matrices for the O_F^- centre in BaFBr.

		Principal direction[a]	
	Principal value	θ (deg)	ϕ (deg)
$\tilde{g}$	$g_1 = 2.0419$	90	0
	$g_2 = 2.0419$	90	90
	$g_3 = 2.0202$	0	–
$\tilde{A}/h(^{17}O)$	$A_1 = 53.42$ MHz	90	0
	$A_2 = 53.42$	90	90
	$A_3 = 271.11$	0	–
$\tilde{A}/h(^{19}F_1)$	$A_1 = -1.86$ MHz	36	135
	$A_2 = -2.46$	54	−45
	$A_3 = 2.25$	90	45
$\tilde{A}/h(^{19}F_2)$	$A_1 = -0.33$ MHz	15	90
	$A_2 = -0.98$	90	0
	$A_3 = 1.94$	105	90
$\tilde{A}/h(^{81}Br)$	$A_1 = 5.538$ MHz	45	−90
	$A_2 = 4.139$	90	0
	$A_3 = 40.882$	45	90
$\tilde{P}/h(^{81}Br)$	$P_1 = 1.623$ MHz	74.5	90
	$P_2 = 0.378$	90	0
	$P_3 = -2.001$	164.5	90

[a] $\theta = \angle(c, \boldsymbol{B})$ and $\phi = \angle[a, c \times \boldsymbol{B} \times c$ (the projection of $\boldsymbol{B}$ onto the ab plane)].

More detailed SHF information was obtained with ENDOR spectroscopy. The ENDOR spectrum obtained with the magnetic field direction 1° from a in the ab plane and a field strength corresponding to the centre of the O_F^- EPR absorption is shown in figure 3. The angular dependences of the transitions in the ab plane are also shown below the a-axis ENDOR spectrum.

The strongest spectral feature in figure 3 appears at a frequency of 13.22 MHz. This frequency is the nuclear Zeeman frequency for ^{19}F (I = 1/2, 100% abundance, $g_N = 5.257732$) at the experimental field strength of 329.68 mT and the line can therefore be assigned to distant ^{19}F ENDOR transitions. The transitions symmetrically disposed about this line in the spectral region 12 to 14.5 MHz also arise from ^{19}F interactions. The angular dependences for this spectral region in the ab and ac planes are shown in detail in figure 4.

Bromine has two naturally occurring isotopes, ^{79}Br (I = 3/2, 50.69% abundance, $g_N = 1.404266$) and ^{81}Br (I = 3/2, 49.31% abundance, $g_N = 1.513706$). For nuclei with spin $I = 3/2$, six allowed first-order ENDOR transitions are expected if there is a quadrupole interaction, three each for the $m_S = \pm 1/2$ electronic spin states

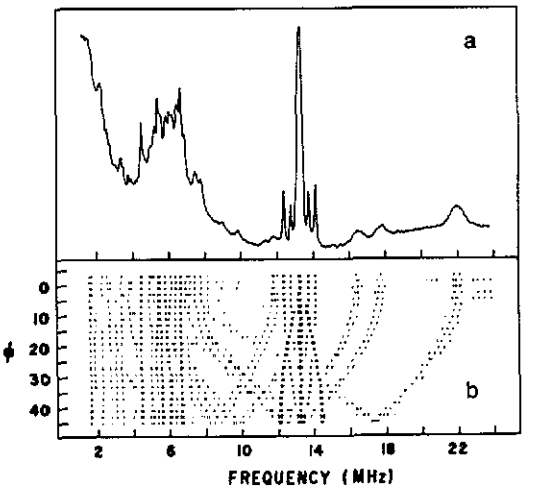

Figure 3. (*a*) ENDOR spectrum ($B \parallel a$, 329.68 mT) of O_F^-. (*b*) Angular dependence in the *ab* plane of O_F^- ENDOR peak positions. As a result of the high RF power necessary to observe the bromine ENDOR lines, harmonics of the fluorine transitions (centered around 13.22 MHz) were observed at lower frequencies (e.g., the isotropic lines at 6.61, 4.41 and 3.31 MHz are harmonics of the fluorine matrix line). The variable parameters in the algorithms used to produce (*b*) were chosen to optimize the resolution of the narrow lines.

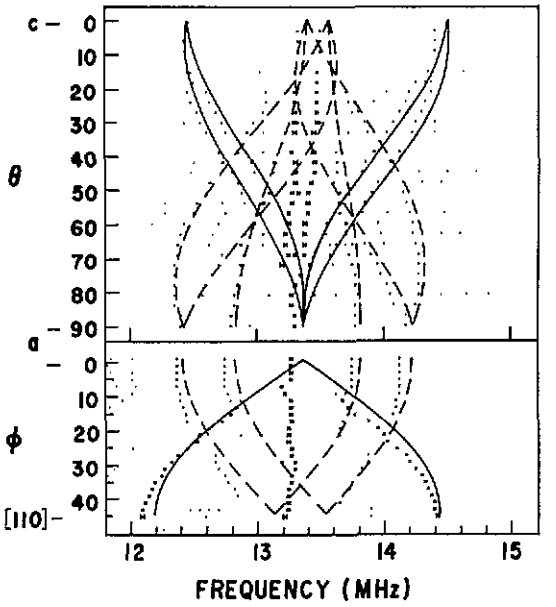

Figure 4. ^{19}F ENDOR transitions of O_F^- in the *ca* and *ab* planes. The dots represent the experimental ENDOR peak positions and the curves represent the transition frequencies calculated from the spin-Hamiltonian matrices (see table 1). The curves were based on EPR transition fields for a fixed microwave frequency (9.5 GHz), rather than on the experimental fields. Solid curves arise from the first shell ions and dashed curves from the second shell ions.

(Köhler *et al* 1990). The energy of the central transition (the so-called 'hyperfine line') for each electronic spin state is not influenced by the nuclear quadrupole interaction to first order. In the ENDOR spectrum of figure 3, a number of weak transitions with similar, broad linewidths are apparent. If the highest frequency line of this set (22.0 MHz) is assumed to be a composite of ^{79}Br and ^{81}Br transitions, then the two lines at 16.4 and 17.8 MHz are the ^{79}Br and ^{81}Br 'hyperfine lines', respectively. Their separation of 1.4 MHz is consistent with the expected isotope shift. Thus, the broad lines are reasonably assigned to bromine transitions.

Numerous transitions at low frequencies (less than 7 MHz), possibly corresponding to interactions with barium ions and more distant bromine neighbours, have not been analysed.

As discussed above, only one symmetry site was observed by EPR for the O_F^- defect. With the caveat that a small site splitting might be missed in the complicated SHF structure, this property requires (Weil *et al* 1973) that the *g*-matrix have either all three principal values equal or, as observed in this case, only two different principal values with the distinct principal direction parallel to the *c*-axis. This form of *g*-matrix implies that O_F^- has four-fold symmetry about a crystallographic four-fold axis and places the O_F^- defect either on a Ba–Br or a F–F four-fold axis (see figure 1).

The qualitative angular dependence of the fluorine ENDOR lines in the *ab* plane (figure 4) can be used to determine which of the four-fold axes passes through the O_F^- defect. If the defect were on the Ba–Br axis, the closest shell of fluoride neighbours would have a defect–F direction which projects along *a* in the *ab* plane. On the other hand, the defect–F directions for the closest fluorides to a defect located on the F–F axis would project onto a [110] direction. The largest observed fluorine interaction in the *ab* plane is along [110], supporting an F–F axis position.

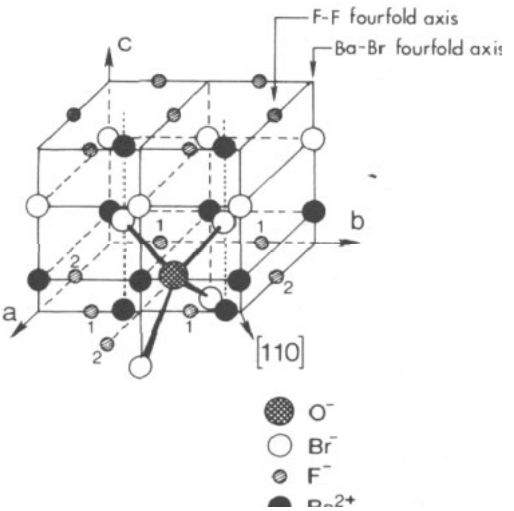

Figure 5. Schematic diagram showing the structure of the O_F^- defect. The fluoride shells surrounding the defect are numbered as referenced in the text.

Based on this model, fluorine ENDOR lines selected from both the *ab* and *ca* plane rotation data sets were assigned as arising from the two shells labelled in figure 5.

The two fluorine hyperfine matrices were each fitted using a spin-Hamiltonian which included only terms for a single fluorine nucleus. Higher order effects such as fluorine–fluorine interactions and the effect of the fluorine nuclei on the electron quantization axis were found to be negligible. ENDOR data for four fluoride ions were included for each shell by using symmetry operations to transform the data to correspond to a single ion. The matrices in table 1 were obtained by fitting 98 transitions for the first shell and 107 transitions for the second shell to mean frequency deviations of 0.044 and 0.045 MHz, respectively. These matrices were used to simulate the fluorine transitions in figure 4. The success of this fit confirms that the defect is on the F–F axis. The principal directions of $A(^{19}F_1)$ and $A(^{19}F_2)$ are used below in conjunction with the bromine SHF data to refine the model of the defect structure. At this point we note that these directions are consistent only with the O^- ion being located in or near the fluoride plane and not with other possible sites, such as the interstitial site half way between F^- ions along the F–F axis.

Using the symmetry properties appropriate for a defect on the F–F axis, 192 ^{81}Br ENDOR lines were selected from both *ab* and *ca* plane rotation data sets and fitted to obtain the bromine SHF and quadrupole matrices with a mean frequency deviation of 0.08 MHz (table 1). As for the fluorine hyperfine fitting, a single bromine interaction was included in the spin-Hamiltonian. The high frequency ^{79}Br and ^{81}Br ENDOR angular dependences in the *ca* plane and the angular dependences simulated from the fitted parameters are shown in figure 6.

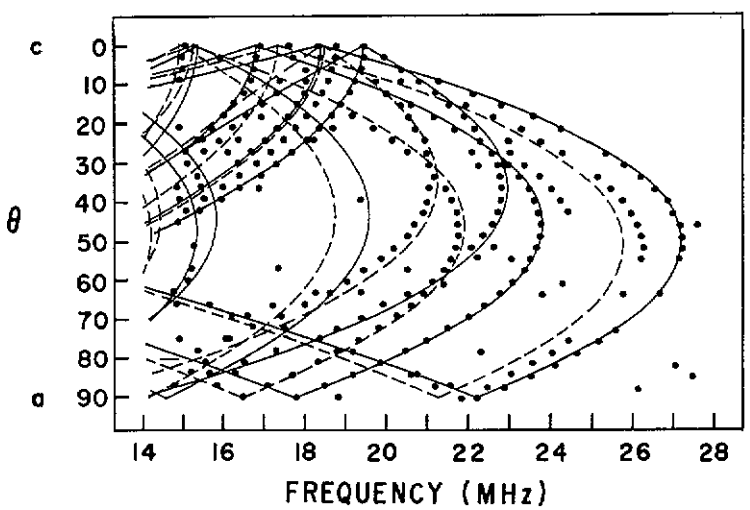

Figure 6. High frequency ^{79}Br and ^{81}Br ENDOR transitions of O_F^- in the *ca* plane. The dots represent the experimental ENDOR peak positions. Solid lines represent ^{81}Br transitions calculated from the ^{81}Br hyperfine matrix in table 1 and dashed lines represent ^{79}Br transitions calculated by scaling the ^{81}Br hyperfine and quadrupole matrices. The calculated transition frequency curves were based on EPR transition fields for a fixed microwave frequency (9.5 GHz), rather than on the experimental fields.

In order to determine the number of equivalent bromide ions giving rise to the fitted ENDOR bromine transitions, the fitted Hamiltonian parameters were used to simulate EPR spectra with the magnetic field parallel to *a*, *c* and [110]. Excellent

agreement between simulated and experimental spectra (figure 2) was obtained only by including four equivalent bromide ions in a single symmetry site. The smaller SHF interactions with other nuclei were taken into account by choosing appropriate linewidths for the simulations. This result shows that the O^- ion is substitutional for F^- and that it remains at the lattice F^- site (figure 5).

An optically detected ENDOR spectrum was measured in the MCDA band of the O_F^- centre at 405 nm (see preceding paper) for $\boldsymbol{B} \parallel \boldsymbol{c}$ at 24 GHz. ENDOR lines were measured in the frequency range between 12 and 28 MHz. ENDOR transitions arising from the nearest bromide neighbours were observed. Their frequency positions agreed with those found in conventional ENDOR for the same field orientation, when allowing for the different nuclear Zeeman frequencies in K band and X band. This confirms once more the assignment of the MCDA bands to the O_F^- centre made in the previous paper by ODEPR. In table 1 the principal values of the SHF matrices and their orientations are collected with the g-matrix, the ^{81}Br quadrupole tensor, and the ^{17}O hyperfine matrix from the previous paper. The isotropic SHF constant a and the anisotropic SHF constants b and b' are related to the principal values by

$$A_1 = a - b + b'$$
$$A_2 = a - b - b'$$
$$A_3 = a + 2b.$$

4. Discussion

An atomistic computation by Baetzold (1990) showed that the lowest energy position for an O^- substituted for fluoride is exactly at the fluoride lattice site, in agreement with our assignment from the analysis of the ENDOR data.

In the preceding paper, it was not possible to satisfactorily explain the g-matrix assuming a simple p_z orbital along the c axis as the electronic ground state of the O_F^- defect. However, within that simple picture it is possible to explain some of the gross features of the SHF interactions. The different signs of a and b for the nearest fluorine neighbours which are in the nodal plane of the p_z orbital are notable and point to the importance of exchange polarization. Therefore, the isotropic and anisotropic SHF constants for the first shell bromide and first and second shell fluoride ions were estimated by considering the following interactions:

$$a = a_{\text{trans}} + a_{\text{pol}}$$
$$b = b_{\text{trans}} + b_{\text{pol}} + b_{\text{dd}}$$
$$a_{\text{trans}} = \frac{2}{3}\frac{\mu_0}{h} g_N \mu_N g_e \mu_B N^2 \mid \Psi(0) \mid^2$$
$$b_{\text{trans}} = \frac{1}{8\pi}\frac{\mu_0}{h} g_N \mu_N g_e \mu_B \int \frac{3z^2 - r^2}{r^5} \mid \Psi(r_n) \mid^2 \mathrm{d}V.$$

The constants μ_0, g_N, g_e, μ_N and μ_B are the permittivity of free space, the nuclear and electronic g-factors and the nuclear and Bohr magnetons, respectively. a_{trans} and b_{trans} are the transferred SHF interactions calculated using the usual one-particle

approximation and an oxide $2p_z$ orbital along the c axis orthogonalized to the appropriate halide ion core as an envelope function (Spaeth and Seidel, 1971). b_{dd} is the dipole–dipole contribution to the anisotropic SHF interaction. a_{pol} and b_{pol} are the contributions arising from exchange polarization of the halide ligands by the unpaired spin on the oxide ion; these will be negative in sign.

Rough estimates of a_{pol} and b_{pol} were made by appropriately scaling terms within the expressions derived previously for Al^{3+}–O^- exchange interactions (equations (10) and (17) in Adrian *et al* 1985) by the ratios of the nuclear g-factors, $|\Psi(0)|^2$ or $\int(3z^2 - r^2/r^5)\,|\Psi(r_n)|^2\,dV$ and the overlap integrals $|<\Psi, ms\,|O^-, 2p_\sigma>|^2$ or $|<\Psi, mp_\sigma\,|O^-, 2p_\sigma>|^2$ for Al^{3+} and Br^- or F^- (m denotes the quantum number of the orbital of the ion, p_σ is the orbital which has its axis along the connection line between the O^- and the neighbour ion). These estimates indicated that for the first shell bromide ions, taking the experimental orientation of the bromine SHF matrix ($\theta = 45°$) instead of the lattice internuclear direction ($\theta = 40.8°$), but using the normal O^-–Br^- lattice distance of 3.44 Å, a_{trans} and a_{pol} are of the same order of magnitude (15.7 and −10.6 MHz, respectively), while b_{pol} is only about 12% of ($b_{trans} + b_{dd}$) (−0.4 and 3.3 MHz, respectively). The calculated values of a and b for a bromide ion in this configuration (5.1 and 2.9 MHz, respectively) are clearly not in good agreement with experiment (16.9 and 12.0 MHz, respectively). Agreement could be obtained by moving the bromide ions toward O^- ($R = 2.3$ Å) and toward the fluoride plane (increasing θ to 56.4°). However, noting the large uncertainties in estimating a_{pol} and b_{pol}, a more accurate picture can probably be obtained by assuming that $b \approx b_{trans}$, using the experimental value for θ of 45° and varying R to give the best agreement with the measured value of b. This gives an O^-–Br^- lattice distance of 2.6 Å. Thus, it is likely that the bromide ions relax toward the oxide defect. A similar argument for the first shell fluoride ions, made assuming that $b \approx b_{dd}$ suggests that the fluoride ions have moved away from the oxide defect (by 0.2 Å). Within the accuracy of the experimental measurements, the second shell fluoride ions remain at the lattice distance of 4.51 Å.

Interactions with the first shell barium ions were calculated to be small and probably account for some of the observed low frequency ENDOR lines which were not analysed.

We can further refine the model for O_F^- by consideration of the principal directions of the fluorine SHF matrices relative to internuclear directions in the BaFBr lattice (see table 1). If we start with the conclusion that the oxide ion does not move from the fluoride site, derived from the result that the four nearest neighbour bromide ions are equivalent to ENDOR precision, then the SHF matrix directions can indicate relaxations of the surrounding lattice to accomodate replacement of fluoride by oxide. The bromide movement discussed above would affect the fluoride positions. The first shell fluoride ions are affected equally by bromide ions above and below the fluoride plane, so they would be expected to remain in this plane, probably moving away from the oxide site. Thus θ for this shell would be expected to be 90°, as was observed. On the other hand, two of the second shell fluoride ions would be expected to move above the fluoride plane and two below the plane in response to the bromide relaxation. To give a 15° angle out of the plane ($\theta = 105°$), as observed, a fluoride movement of about 1.2 Å along c would be required. Although this estimate of the distortion seems rather large, it is near to the relaxation of 0.9 Å estimated for bromide above. The inward movement and contraction toward the fluoride plane of the bromide ions, the outward movement of the first shell fluoride ions and the "rippling" of the second

shell fluoride ions are all consistent with the type of relaxations predicted by atomistic defect calculations (Baetzold 1990) using parameters and potentials that have given realistic results in past studies (Baetzold 1987, 1989), although the agreement is only qualitative.

In the preceding paper, we discussed a possible explanation for the experimental g-matrix based upon a motion of the O_F^- centre that causes appreciable positive deviations of the three principal values from 2. The observation of the large effects of exchange polarization on the isotropic hyperfine constant of the nearest fluorine neighbours, however, shows that such a motion must preserve, to a large extent, the p_z character along the c axis. Since the ionic radius of O^- is much smaller than that of F^-, an off-centre position for O^- seems possible. However, the observed equivalences of the fluoride and bromide neighbours in ENDOR implies that if such a model obtains, rapid motion of the O^- ion about the c axis must occur. Such a motion would also reduce the observable anisotropic part of the ^{17}O hyperfine interaction by partial motional averaging. A contribution from dynamics would explain the low $2p_z$ orbital occupancy estimated in the previous paper and would be consistent with the inability of Hartree–Fock calculations based on a rigid model to predict this occupancy (Baetzold obtained a value close to 0.99).

5. Summary

A trapped-hole species in BaFBr has been identified as O_F^-, an oxygen ion substituted at a fluoride site. The lattice relaxation of the defect does not include any movement of the O^- from the F^- site, but does involve movement of the nearest bromide neighbours toward the oxide and toward the fluoride plane and a corresponding movement of the second shell fluoride neighbours out of the plane. No evidence has been found for the presence of a neighbouring defect (anion vacancy or interstitial cation) remaining from its charge-compensating role in the proposed O_F^- precursor species.

Acknowledgments

We thank H Luss for the Laue back reflection measurements. J A Weil (University of Saskatchewan) kindly provided the computer program used to fit the spin-Hamiltonian parameters. We thank J *R* Niklas for his many contributions to the development of both the hardware and software for our ENDOR facility. We have particularly benefited from extensive discussions with *R* Baetzold and M S Islam, and from access to the results of their calculations prior to publication.

References

Adrian F J, Jette A N and Spaeth J-M 1985 *Phys. Rev.* B **31** 3923
Ahlers F J, Lohse F and Spaeth J-M 1982 *Solid State Commun.* **43** 321
Baetzold R C 1987 *Phys. Rev.* B **36** 9182
—— 1989 *J. Phys. Chem. Solids* **50** 915
—— 1990 private communication
Beck H P 1979 *Z. Anorg. (Allg.) Chem.* **45** 173
Eachus R S and Nuttall R H D 1988 *Int. Conf. on Defects in Insulating Crystals (Parma, Italy, 1988)* Paper summaries p 223

Eachus R S, McDugle W G, Nuttall R H D, Olm M T, Koschnick F K, Hangleiter Th and Spaeth J-M 1991 *J. Phys.: Condens. Matter* **3** 9327

—— 1991b in preparation.

Hangleiter T, Koschnick F K, Spaeth J-M, Nuttall R H D and Eachus R S 1990 *J. Phys.: Condens. Matter* **2** 6837

Köhler K, Kirmse R, Böttcher R, Abram U, Gribnau M C M, Keijzers C P and de Boer E 1990 *Chem. Phys.* **143** 83

Koschnick F K, Söthe H and Spaeth J-M 1988 *Int. Conf. on Defects in Insulating Crystals (Parma, Italy, 1988)* Paper summaries p 149

Koschnick F K and Spaeth J-M 1991 to be published

Liebich B W and Nicollin D 1977 *Acta Crystallogr.* B **33** 2790

Meyer B K, Heder G, Lohse F and Spaeth J-M 1982 *Solid State Commun.* **43** 325

Niklas J R 1983 *Habilitationsschrift* Universität-GH Paderborn

Rinneberg H and Weil J A 1972 *J. Chem. Phys.* **56** 2019

Spaeth J-M 1989 *Electron Spin Resonance* vol 11B, ed M C R Symons (London: Royal Society of London) p 89

Spaeth J-M and Seidel H 1971 *Phys. Status Solidi* b **46** 323

Spoonhower J P and Ahlers F J 1989 unpublished results

Takahashi F, Kohda K, Miyahara J, Kanemitsu Y, Amitani K and Shionoya S 1984 *J. Lumin.* **31&32** 266

Takahashi K, Miyahara J and Shibahara Y 1985 *J. Electrochem. Soc.* **182** 1492

Trauernicht D P and Sever B R 1988 unpublished results

von Seggern H 1988 *Int. Conf. on Defects in Insulating Crystals (Parma, Italy, 1988)* Paper summaries p 311

von Seggern H, Voigt T, Knüpfer W and Lange G 1988 *J. Appl. Phys.* **64** 1405

Weil J A, Buch T and Clapp J E 1973 *Adv. Mag. Res.* **6** 183